Available online at www.sciencedirect.com

Chemical Engineering Research and Design

journal homepage: www.elsevier.com/locate/cherd

Design and simulation of reverse osmosis process in a hybrid forward osmosis-reverse osmosis system

S.U. Sayyad[a,*], N.K. Kamthe[a], S.M. Sarvade[b]

[a] Civil and Environmental Engineering Department, VJTI, Mumbai, MH, India
[b] Department of Civil Engineering, Dr. B.A.T.U, Vidyavihar, Lonere, MH, India

ARTICLE INFO

Article history:
Received 26 February 2022
Received in revised form 1 May 2022
Accepted 5 May 2022
Available online 10 May 2022

Keywords:
Hybrid FO-RO system
Draw solution regeneration
Reverse Osmosis
Multi element design
Python

ABSTRACT

Reverse Osmosis (RO) is one of the widely adopted methods for water desalination to mitigate shortage of freshwater for domestic, irrigation and industrial consumption. Recently RO is also used as a draw solution regeneration step for most hybrid Forward Osmosis-Reverse Osmosis (FO-RO) systems used for water desalination. Accurate model is required which is more flexible and reliable, to design and operate RO treatment plants for producing freshwater from various water resources. However, most models do not represent multi element field scale RO systems accurately. Plant engineers widely use the available commercial programs for the design of multi element RO systems where the computational code is not provided, which makes the program inflexible. This work presents a computational tool developed on the python platform for the prediction and analysis of the RO process employed in a hybrid FO-RO system. A steady state model based on the solution-diffusion and film theory is established by employing concentration polarization, pressure drop and average solution properties in the computational calculations of the RO process. The model is used to design and estimate the performance parameters of an entire RO system having multiple membrane elements installed in a pressure vessel. A comparison between the outputs obtained by the model and membrane manufacturers software shows good agreement.

1. Introduction

Amongst several technologies for desalination, Reverse Osmosis (RO) is the most commonly and actively adopted technique for seawater desalination (Pais and Ferreira, 2007; Liang et al., 2021), groundwater desalination (Brião et al., 2014), surface water treatment (Cornelissen et al., 2021), municipal (Lakho et al., 2021; Qin et al., 2005) and industrial wastewater (Al-Obaidi et al., 2021) treatment. This technology is used to generate water not just for drinking or domestic use (Joshi et al., 2004; Askari et al., 2021) but also for industrial (Colla et al., 2016; Jeong et al., 2021) and irrigation purposes (Rahimi et al., 2021). However fluctuations in the feedwater source (Ruiz-García et al., 2020), fouling (Lee et al., 2010; Melián-Martel et al., 2018), scaling (Zaviska et al., 2015), boron removal (Park et al., 2012), performance decline over long time periods (Ruiz-García and Nuez, 2016) and high energy consumption (Zaviska et al., 2015) in the RO systems are the problems which limit the utilization of this technology. Fabricating novel RO membranes with good scaling and fouling resistance is important for successful application of RO systems (Hao et al., 2021). Conventional and Membrane based RO feedwater pretreatment methods are adopted to prolong the life of RO systems (Jamaly et al., 2014).

Recently the Forward Osmosis (FO) process also has been considered as an efficacious pretreatment method to RO process which improves the overall performance of RO process (Choi et al., 2016). The concept of FO pretreatment of raw

* Corresponding author.
E-mail address: susayyad@ci.vjti.ac.in (S.U. Sayyad).
https://doi.org/10.1016/j.cherd.2022.05.002

Nomenclature

Description Notation (Unit)
Total membrane area A_m (m^2)
Water permeability constant at operating temperature A_T ($m/s.Pa$)
solute permeability of the feedwater B (m/s)
breadth of the membrane b (m)
average of the feed and brine concentration C ($Moles$)
permeate water concentration C_p (mg/L)
Concentration polarization modulus CP
feed water concentration C_f (mg/L)
Concentration factor CF
solute diffusivity coefficient for Sodium Chloride solution D (m^2/s)
diffusion coefficients of sodium ion at temperature T in kelvin $D_{Na,T}$
diffusion coefficients of chloride ion at temperature T in kelvin $D_{Cl,T}$
filament thickness df (m)
hydraulic diameter dh (m)
Forward osmosis FO
i^{th}, Pressure vessel or pressure vessel number i
total water flux Jw ($m^3/m^2.s$)
Element number or j^{th} membrane element j
mass transfer coefficient k (m/s)
pressure vessel & module fitting losses in pressure vessel K_λ
length of the membrane element L (m)
mesh length l_m (m)
Total number of membrane elements in each pressure vessel N
number of membrane envelopes in one spiral wound module n
Total number of pressure vessel N_{pv}
feed water pressure in RO system P_f ($kg/m.s^2$)
permeate hydraulic pressure P_p ($kg/m.s^2$)
net applied hydraulic pressure in RO ΔP ($kg/m.s^2$)
pressure drop at the feed side of the spiral wound membrane ΔP_{fb} ($kg/m.s^2$)
Rate of flow of RO concentrate Q_c (m^3/s)
Rate of flow of RO feed water Q_f (m^3/s)
Rate of flow of RO permeate water Q_p (m^3/s)
Reynolds Number Re
Reverse osmosis RO
Recovery R
Schmidt Number Sc
Specific energy consumption SEC (kWh/m^3)
Temperature T (°C or Kelvin)
velocity of average feed and concentrate solution V_{fb} (m/s)
feed spacer volume V_{sp} (m^3)
feed channel volume V_{total} (m^3)

Description Greek letters (Unit)
porosity ε
density of sodium chloride solution ρ (kg/m^3)
density of pure water ρ_w (kg/m^3)
dynamic viscosity of sodium chloride solution μ ($kg/m.s$)
water dynamic viscosity $\mu_{w,T}$ $kg/m.s$
feedwater osmotic pressure Π_f ($kg/m.s^2$)
Permeate water osmotic pressure Π_p ($kg/m.s^2$)
osmotic pressure of the average feed and brine concentration at the surface of the active layer of RO membrane Π_m ($kg/m.s^2$)
difference in the osmotic pressure of the solution across the membrane selective layer $\Delta\Pi$ ($kg/m.s^2$)

Description Subscripts
Concentrate water c
feed water f
feed & brine fb
membrane m
permeate water p
spacer sp

water is like the concept of UF/MF membrane pretreatment prior to the RO desalination process. Such a system is called a hybrid Forward Osmosis-Reverse Osmosis (FO-RO) system as shown in Fig. 1. The FO membrane represents an effective barrier for removal of not only suspended solids and micro-organisms but also of a range of dissolved solids that represent a fouling and scaling threat to the RO system (Bamaga et al., 2011). Also, the FO membranes are less susceptible to fouling due to low operating pressure operation (McCutcheon et al., 2006). The role of RO in the hybrid FO-RO system is to regenerate the draw solution used in the FO process. Many FO-RO experimental ((Yangali-Quintanilla et al., 2011; Bowden et al., 2012; Thiruvenkatachari et al., 2016; Ali et al., 2016; Choi et al., 2016; Chun et al., 2016)) and real studies (Al-Zuhairi et al., 2015) have been reported while few FO-RO studies employ experimental (for FO studies) and/or simulation approaches (for FO and RO) to provide the performance efficiency of FO-RO systems. Review on the latter approach is discussed below.

Achilli et al. (2010) studied on finding optimum draw solution from a set of 14 different draw solutions for FO-RO systems. Authors conducted experiments on FO process only and employed RO simulation softwares for predicting the performance of RO process for draw solution regeneration. Using the softwares Reverse Osmosis System Analysis (ROSA) (Dow Filmtec, Midland, MI) and IMSDesign (Hydranautics, Oceanside, CA) the performance of RO for re-concentration of each draw solution was evaluated in terms of RO permeate concentrations. All simulations were performed using five RO membrane elements in series, at a feed flow rate of 3.0 m^3/h, and with a system recovery of 35%. The draw solutions were tested at a feed osmotic pressure of 2.8 MPa and a temperature of 25 °C. When sodium chloride solution of concentration 35.2 g/L was used as the RO feedwater solution, the resulting RO permeate concentration given by ROSA and IMS Design was 127.3 mg/L and 179 mg/L respectively (Jeon et al., 2016) in his study conducted simulation of hybrid FO-RO system and employed RO simulation software ROSA (DOW, Filmtec, USA) for the performance prediction of RO process. The input data for the ROSA RO simulation software are diluted draw solution (seawater) as RO feedwater concentration, RO product flow rate, RO permeate flux, RO recovery rate, RO element type, number of elements per pressure vessel (PV), and the PV arrangements. For single stage (8 elements per pressure vessel and 10 pressure vessels in parallel) RO system with RO feed flow rate of 2000 m^3/day, RO feed water concentration of 35000 mg/L, RO feedwater temperature of 25 °C and RO recovery rate of 50%, the software calculated hydraulic pressure and RO

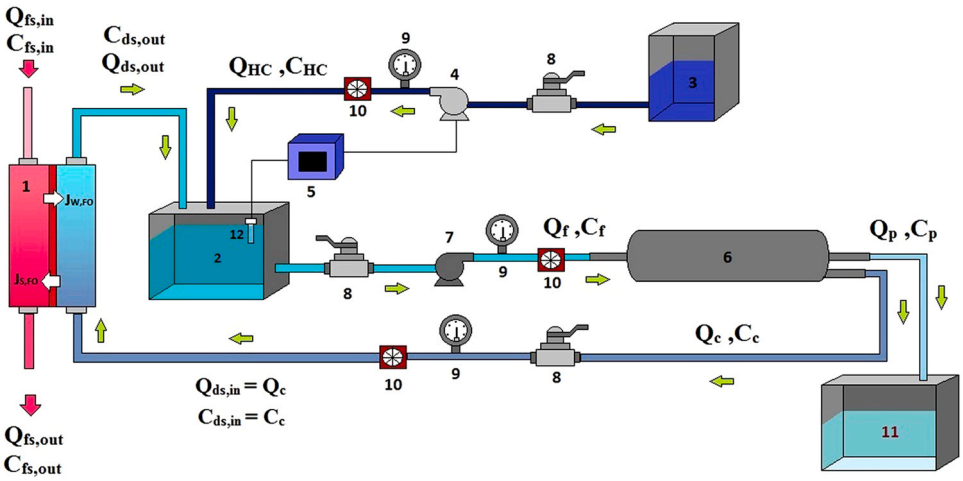

Fig. 1 – Hybrid Forward Osmosis- Reverse Osmosis System. 1: Forward osmosis unit, 2: Diluted draw solution tank, 3: High concentration draw solution reservoir, 4: Dosing pump, 5: Conductivity controller unit, 6: Reverse osmosis unit, 7: High pressure pump, 8: Flow control valve, 9: Pressure gauge, 10: Inline flow meter, 11: Permeate Tank, 12: Conductivity probe.

permeate concentration was 56.61 bars and 237.54 mg/L respectively. Similarly, Altaee et al. (2017) in his study of finding energy efficiency of an FO-RO system, has employed a modeling approach for predicting process performance of FO while employing ROSA 9.1 for simulating performance of RO process. The RO process performance is simulated for 4 m^3/h RO feed flow rate, RO recovery rate of 46%, 40% and 38% for RO feed water concentration of 35, 40 and 45 g/L of sodium chloride solution respectively and RO membrane configuration having single stage, single pressure vessel with 8 elements in a single pressure vessel. For the RO step of the FO-RO system the flux decline was considered to be equal to that of a second pass of dual-pass RO process whereas the silt density index (SDI) of the RO step in the FO-RO system was considered to be less than 1. For the RO step of the FO-RO systems without energy recovery devices the specific energy consumption values were 4.32, 4.89 and 5.8 kWh/m3 for 35, 40 and 45 g/L seawater salinities respectively.

Many commercial software programs are available for the design and estimation of a RO process (Mancha et al., 2014). These softwares provide wide information on the membrane element wise performance of the multielement RO system. But these software's make certain assumptions and use the same equation required for feed water characterization for all types of RO feed water entering the RO system. Essentially this may not be correct in situations where RO application is for draw solution regeneration in a FO-RO hybrid system where the draw solution is mostly a binary feed solution like NaCl, KCl and $CaCl_2$ (Khraisheh et al., 2020). Moreover, these commercial software's do not enable users to use membranes other than those supplied by the membrane manufacturer (Altaee, 2012). The membrane manufacturers also impose constraints in the software on parameters like minimum RO concentrate flow rate, maximum RO Permeate flow rate and RO feed flow rate which cannot be changed by the user (Ruiz-García and Nuez-Pestana, 2018). Inadequacies in commercial programs for the design of RO systems stimulate the creation of new ones that allow for more flexible design and more realistic operating circumstances for these types of systems. Researchers have proposed the design and modeling of the multielement RO system.

Nafey et al. (2006) developed a computational model using visual basic language for design and simulation of multi element reverse osmosis process. Authors considered single stage RO system arrangements with 7 membrane elements in each pressure vessel and 42 pressure vessels, RO feed flow rate of 486 m^3/h, RO feedwater temperature between 25 °C and 40 °C, RO recovery of 30% for a RO feed water concentrations of 45000 mg/L. These input parameters were of an existing reverse osmosis desalination plant which were used to run the computational model. The results of the computational model were compared with reverse osmosis software program 'ROSA'. The computational model results were in good agreement with 'ROSA', with only 7% lower estimation of feedwater pressure and 2% higher estimation of permeate concentration as compared to ROSA. Altaee (2012) developed a computational model for multielement RO system design and performance. Author considered single stage RO system arrangements with 4 membrane elements in each pressure vessel, RO feed flow rate of 4 m^3/h, RO system temperature of 25 °C, RO recovery of 30% for a RO feed water concentrations of 35 g/L and 38 g/L sodium chloride solutions respectively. Author provided a systematic procedure for estimating performance of each membrane element in the RO system in terms of RO permeate concentration (mg/L), RO applied hydraulic pressure (bars) and RO permeate flow rate (m3/h) and compared the model performance with commercial RO software ROSA. The model developed can be used for any type of membrane which needs to be investigated. Finally, the output of the model is compared with a commercial RO design software and is not experimentally validated. Ruiz-García and Nuez-Pestana (2018) developed an algorithm for designing RO systems. The algorithm is more efficient than the commercial software (ROSA) supplied by membrane manufacturers. The results of the algorithm for design of RO systems were compared with 4 existing RO plants and ROSA software for validation purposes. The algorithm results were more near to the real results of the 4 existing RO plants as compared to results provided by ROSA.

The aim of this work is to develop an algorithm to design the RO step of the FO-RO hybrid system. This work uses the python programming language to simulate the performance of multiple spiral wound RO elements in a pressure vessel of a single stage RO system used for draw solution regeneration in a FO-RO hybrid system. Application of RO for regeneration

Table 1 – Constants in the reverse osmosis process. [adapted from (Eddouibi et al., 2021) with permission].

SN	Parameter	Unit	Value
1	Diffusion coefficient of sodium ion at 298 Kelvin ($D_{Na,\ 298}$)	m^2/s	1.334×10^{-9}
2	Diffusion coefficient of chloride ion at 298 Kelvin ($D_{Cl,\ 298}$)	m^2/s	2.032×10^{-9}
3	Dynamic viscosity of water at 298 Kelvin ($\mu_{w,\ 298}$)	kg/m.s	8.9322×10^{-4}

of draw solution in a FO-RO system is considered to be new. The draw solution from the FO unit outlet is the feed solution to RO unit. Authors have considered sodium chloride solution as the draw solution. Authors have calculated density, viscosity and diffusivity with respect to sodium chloride solution. In the commercial RO softwares these parameters are not displayed. Neither any of the RO model from literature nor any commercial RO softwares provide correct estimation of above parameters because they use a general equation for feedwater characterization to the best of authors knowledge. This is considered as novel in the design steps for RO having application of regenerating the sodium chloride solution used as the draw solution in the FO process. Further, to the best of authors knowledge, the implementation of python programming language for the design of multiple spiral wound RO elements in a pressure vessel of a single stage RO system is not found in literature. This computational tool allows the user to choose any type of RO membrane, regardless of its manufacturer. Furthermore, the model can design multi-element multi pressure vessel single stage RO systems under varying temperature and feed solution (sodium chloride) concentrations. Finally, the performance of the RO process in terms of recovery ratio, salt rejection and specific energy consumption is compared to those obtained from the commercial RO software (Toray, 2021).

2. Materials and methods

2.1. Reverse osmosis system model assumptions

The following assumptions were made to develop the RO process in a hybrid FO-RO system.

a. There is a continuous gradient in chemical potential from one side of the membrane to the other (Wijmans and Baker, 1995).
b. As per Solution Diffusion model no pressure gradient exists within the membrane and the pressure within a membrane is uniform. The chemical potential gradient across the membrane is expressed only as a concentration gradient. Chemical potential of the feed and permeate fluids are in equilibrium with the adjacent membrane surfaces (Wijmans and Baker, 1995).
c. The RO membrane is a homogeneous, non porous surface layer.
d. The feed and permeate channel at the spiral wound membrane module are considered to be flat (negligible curvature), since the thickness of the channels is much lower than the radius of the module (Dimitriou et al., 2017).
e. The RO process is an isothermal process, meaning constant temperature at the feed and permeate channels (Al-Obaidi et al., 2018).
f. The concentration polarization is quantified by the film theory model (Al-Obaidi et al., 2018).
g. At the feed (or brine) and permeate channel, the solute concentration, the fluid velocity and pressure do not vary in the spiral direction (1-D model). A steady state plug flow is considered inside the feed channel and concentration variation in perpendicular direction is neglected (Dimitriou et al., 2017).
h. The salt feed water stream of RO system is sodium chloride solution having concentration of 22,784.6 mg/L.
i. The pressure drop at the permeate side is negligible, so a constant permeate pressure is assumed (101.3 kPa) (Al-Obaidi et al., 2018).

2.2. Model equations and description

Solution Diffusion Model is widely used to model the transport of solvent and solute through an RO membrane. In this model, the total water flux Jw, ($m^3/m^2.s$) is as given by Fritzmann et al. (2007) in Eq. (1).

$$J_w = A_T\,(\Delta P - \Delta\Pi) \tag{1}$$

where A_T is the water permeability constant at operating temperature (°C), (m/s.Pa), ΔP is the difference in the applied hydraulic pressure across the membrane ($kg/m.s^2$) and ΔΠ is the difference in the osmotic pressure of the solution across the membrane selective layer ($kg/m.s^2$). The temperature is one of the important factors which affects the RO process. The water permeability constant A_T at any temperature may be estimated by applying Temperature Correction Factor (TCFp) to the intrinsic water permeability constant, $A_{25\,°C}$ for the permeate as given by Al-Obaidi et al. (2018) in the Eqs. (2) and (3).

$$A_T = A_{25°C} \times exp\,[0.0343(T - 25)] < 25°C \tag{2}$$

$$A_T = A_{25°C} \times exp\,[0.0307(T - 25)] > 25°C \tag{3}$$

ΔΠ is calculated as given in Eq. (4).

$$\Delta\Pi = \Pi_m - \Pi_p \tag{4}$$

where Π_m is the osmotic pressure of the average feed and brine concentration at the surface of the active layer of the RO membrane and is given by Eq. (5) and Π_p is the RO permeate osmotic pressure ($kg/m.s^2$).

$$\Pi_m = CF \times CP \times \Pi_f \tag{5}$$

In Eq. (5) Π_f is the feedwater osmotic pressure ($kg/m.s^2$) which is calculated by the using Eq. (6) as given by Al-Obaidi et al. (2019). The Eq. (6) is used here to calculate the osmotic pressure of feedwater at any temperature T (°C) for known feedwater concentration C_f (mg/L).

$$\Pi_f = 79.94 \times C_f[1 + 0.03(T - 25)] \tag{6}$$

In Eq. (5) CP (unitless) is the concentration polarization modulus (Jiang et al., 2014) and is given by Eq. (7).

$$CP = exp\left[\frac{J_w}{k}\right] \tag{7}$$

Table 2 – Operating conditions of RO process used by Model and Toray software.

SN	Parameter	Unit	Value
1	RO Plant Feedwater Flow Rate ($Q_{f,\ plant}$)	m^3/s	225,000
2	Feedwater Concentration (C_f)	mg/L	22,784.6
3	Feedwater Temperature (T)	°C	15, 20, 25, 30, 35
4	RO plant Recovery ratio (R_{plant})	unitless	0.6722
5	Flow Factor (F_f)	unitless	0.977
6	Pump efficiency (η_p)	unitless	0.8
7	Motor efficiency (η_m)	unitless	1.0
8	Number of Pressure vessels (N_{pv})	nos	08
9	Number of elements in one pressure vessel (N)	nos	10

Eq. (7) is based on the film theory model where it is assumed that a thin layer of unmixed solution exists between the active layer of the membrane surface and the bulk solution. The buildup of the solute concentration in the unmixed layer is termed as concentration polarization. The mass transfer coefficient k (m/s) through the membrane for a spiral wound RO module is computed as per Eq. (8) given by Koroneos et al. (2007).

$$k = 0.065 \times \frac{D}{dh} \times Re^{(0.875)} \times Sc^{(0.25)} \tag{8}$$

Where D is the solute diffusivity coefficient (m^2/s) for sodium chloride solution, dh is the hydraulic diameter (m) of the spiral wound RO module, Re is the Reynolds number, Sc is the Schmidt Number. The solute diffusivity coefficient for sodium chloride D (m^2/s), is evaluated from the Eq. (9) given by Eddouibi et al. (2021).

$$D = \frac{2}{\frac{1}{D_{Na,T}} + \frac{1}{D_{Cl,\ T}}} \tag{9}$$

The diffusion coefficients of sodium and chloride ions are influenced by temperature and viscosity of the solution. To account for the impact of both these factors, the diffusion coefficients of sodium and chloride ions are expressed in terms of temperature (°K) and dynamic viscosity (kg/m.s) and are given by Eqs. (10) and (11).

$$D_{Na,\ T} = D_{Na,298} \times \frac{T}{298} \times \frac{\mu_{w,\ 298}}{\mu_{w,T}} \tag{10}$$

$$D_{Cl,\ T} = D_{Cl,\ 298} \times \frac{T}{298} \times \frac{\mu_{w,\ 298}}{\mu_{w,T}} \tag{11}$$

In Eqs. (10) and (11) the $D_{Na,\ 298}$, $D_{Cl,\ 298}$ and $\mu_{w,\ 298}$ are constants given in Table 1. The water dynamic viscosity, $\mu_{w,T}$ (kg/m.s) at any temperature is calculated as per Eq. 12 given by Eddouibi et al. (2021).

$$\mu_{w,T} = \frac{(T - 273.15) + 246.0}{(0.05594(T - 273.15) + 5.2842)(T - 273) + 137.37} \tag{12}$$

In Eq. (8), dh is the hydraulic diameter (m), which is a spiral wound membrane module characteristic and is given by Eq. (13) as per (Shock and Miquel, 1987).

$$dh = \frac{4 \times \varepsilon}{\frac{2}{h} + (1 - \varepsilon)\frac{4}{d_f}} \tag{13}$$

$$\varepsilon = 1 - \frac{V_{sp}}{V_{total}} \tag{14}$$

$$V_{sp} = 0.5 \times \Pi \times d_f^2 \times l_m \tag{15}$$

$$V_{total} = l_m^2 \times sin\theta \times h \tag{16}$$

where ε is the porosity (unitless), h is the feed spacer thickness (m), d_f is the filament thickness (m), θ is the feed spacer angle (degrees), V_{sp} is the feed spacer volume (m^3) and V_{total} is the feed channel volume (m^3). In Eq. (8) Re is the Reynolds Number and Sc is the Schmidt Number. The Reynolds Number and the Schmidt Number are given by Eq. (17) and Eq. (18) respectively.

$$Re = (\rho \text{ x } V_{fb} \text{ x } dh) / \mu \tag{17}$$

$$Sc = \mu / (\rho \text{ x } D) \tag{18}$$

Where ρ is the density of sodium chloride solution (kg/m^3), V_{fb} is the average velocity of feedwater and brine water in the feed channel (m/s) and μ is dynamic viscosity (kg/m.s) of the sodium chloride solution. The density of sodium chloride solution at any temperature T (°Kelvin) is given by Eq. (19) adapted from (Eddouibi et al., 2021).

$$\rho = \rho_w + (0{\cdot}4485 \text{ x } 10^2 \text{ x } C) - [9{\cdot}634 \text{ x } 10^{-2} \text{ x } C\ (T - 273)] + [0{\cdot}6136 \text{ x } 10^{-3} \text{ x } C\ (T - 273)^2] - 2{\cdot}712 \text{ x } C^{1.5} + [1{\cdot}009 \text{ x } 10^{-2} \text{ x } C^{1.5} (T - 273)] \tag{19}$$

where, ρ_w is the density of pure water (kg/m^3) and ρ_w at any temperature T (°Kelvin) is expressed as given in Eq. (20) and C is the average of the feed and brine concentration (M) as given by Eq. (21) adopted from Eddouibi et al. (2021).

$$\rho_w = 999{\cdot}65 + [2{\cdot}043810^{-1} \text{ x } (T - 273{\cdot}15)] - [6{\cdot}17410^{-2} \text{ x } (T - 273{\cdot}15)^{1.5}] \tag{20}$$

$$C = [(2 - R) \text{ x } C_f] / [(2 - 2\,R) \text{ x } MW_{NaCl}] \tag{21}$$

In Eq. (21), R is the recovery which is given by Eq. (22).

$$R = Q_p/Q_f \tag{22}$$

Where, Q_p is the RO permeate flow rate (m^3/s), and Q_f is the RO feedwater flow rate (m^3/s). The dynamic viscosity of sodium chloride solution, μ, (kg/m.s) at any temperature T (Kelvin) is given by Eq. (23) adapted from Eddouibi et al. (2021).

$$\mu = e^{\frac{16.22\times[MW_{NaCl}\left(\frac{C}{\rho}\right)^{1.3299}+1.4849}{(7.4691107^{-3}(T-273.15)+1)\ \times[30.78(MW_{NaCl}\left(\frac{C}{\rho}\right))^{2.0583}+1]}} \tag{23}$$

where in Eqs. (21) and (23), MW_{NaCl} is the molecular weight of sodium chloride. In Eq. (17) V_{fb} is the velocity of average feed and concentrate solution (m/s) and is given by Eq. (24) (Gaublomme et al., 2020).

Table 3 – Membrane element specifications and configuration used by Model and Toray software. [adapted from Al-Obaidi et al. (2019) with permission].

SN	Item	Value	
1	Membrane manufacturer	Toray	
2	Membrane element designation	TM820M-400/SWRO	
3	Total active area of membrane (Am)	m^2	37.3
4	Length of membrane element (L)	m	1
5	Breadth of the membrane (b)	m	37.3
6	Filament thickness (d_f)	m	0.0004818
7	Length of mesh (l_m)	m	0.00277
8	Spacer thickness (h)	m	0.0008636
9	spacer Angle (θ)	degrees	129
10	Number of envelopes (n)	nos	1
11	Intrinsic water permeability constant at 25 °C	m/s.Pa	3.16×10^{-12}
12	Intrinsic solute permeability constant at 25 °C	m/s	1.75×10^{-8}
13	Maximum element recovery (R_{max})	%	30
14	Maximum feed flow rate per element ($Q_{f,\ max}$)	m^3/s	4.56×10^{-3}
15	Minimum Brine flow rate per element ($Q_{c,\ min}$)	m^3/s	6.31×10^{-4}

$$V_{fb} = (Q_f + Q_c) / [2 \text{ x } (b \text{ x } n \text{ x } \varepsilon \text{ x } h)] \quad (24)$$

where, in Eq. (24), Q_c is the RO concentrate flow rate (m^3/s), b is the breadth of the membrane (m), n is the number of membrane envelopes in one spiral wound module.

In Eq. (4) Π_p is the Permeate water osmotic pressure (kg/m.s^2) which is calculated by the using Eq. (25) as given by Al-Obaidi et al. (2019). The Eq. (25) is used here to calculate the osmotic pressure of permeate water at any temperature T (℃) for known permeate water concentration C_p (mg/L).

$$\Pi_p = 79.94 \times C_p \quad [1 + 0.03(T - 25)] \quad (25)$$

The permeate water concentration Cp (mg/L) is calculated using Eq. (26) as given by Ruiz-García and Nuez-Pestana (2018).

$$C_p = B \text{ x } CP \text{ x } (A_m / Q_p) \text{ x } [C_f \text{ x } (1 + CF) / 2] \quad (26)$$

where, A_m is the net effective membrane area (m^2) provided for the RO system and B is the solute permeability of feedwater (m/s). The solute permeability of the feedwater is dependent on the temperature of the feedwater and temperature correction factor is applied to intrinsic solute permeability coefficient B_{25}, as given in Eqs. (27) and (28) to obtain B (Al-Obaidi et al., 2019).

$$B = B_{25} \text{ x } [1 + 0.05\ (T - 25)] \text{ for } T < 25 \quad (27)$$

$$B = B_{25} \text{ x } [1 + 0.08\ (T - 25)] \text{ for } T > 25 \quad (28)$$

In Eq. (1) ΔP is the net applied hydraulic pressure (kg/m.s^2) to the RO system and is given by Eq. (29).

$$\Delta P = P_f - (\Delta P_{fb} / 2) - P_p \quad (29)$$

where, P_f is feedwater pressure (kg/m.s^2) in the RO system and ΔP_{fb} is the pressure drop at the feed side of spiral wound membrane (kg/m.s^2). P_p is permeate hydraulic pressure (kg/m.s^2) and is considered negligible.

The pressure drop at the feed side of the spiral wound membrane ΔP_{fb} (kg/m.s^2) is calculated using Eq. (30) (Jiang et al., 2014).

$$\Delta P_{fb} = \frac{\lambda L \rho \quad (V_{fb})2}{2dh} \quad (30)$$

where, λ is empirical friction factor, L is the length of the membrane element (m) and ρ is the density of sodium chloride solution (kg/m^3). In Eq. (30), the empirical friction factor λ is given by Eq. (31) (Ruiz-García and de la Nuez Pestana, 2019).

$$\lambda = K_\lambda \times 6.23 \times Re^{-0.3} \quad (31)$$

K_λ is a factor taking into consideration the additional pressure losses in the feed of the PVs and module fittings. Its value lies in between 1.9 and 2.9 and is 2.4 in this study. Water flow through the RO membrane can be determined by the following equation (Ruiz-García and Nuez-Pestana, 2018) considering the flow factor (F_f).

$$Qp = F_f \text{ x } A_T \text{ x } (\Delta P - \Delta \Pi) \text{ x } S_m \quad (32)$$

Rearranging and writing Eq. (32) in terms of applied hydraulic pressure P_f (kg/m.s^2) to the RO feedwater gives.

$$P_f = [Q_p / (A_T \text{ x } F_f \text{ x } S_m)] + \Delta \Pi + (\Delta P_{fb} / 2) \quad (33)$$

Finally, the specific energy consumption SEC, (kWh/m^3) given by (Al-Obaidi et al., 2019) is calculated by Eq. (34) as given below.

$$SEC = P_f / (\eta_p \text{ x } \eta_m \text{ x } R \text{ x } 1000 \text{ x } 3600) \quad (34)$$

Where η_p and η_m are the pump and motor efficiency respectively.

The equations from (1) to (34) explain the steps to model the reverse osmosis process with the spiral wound membrane module.

2.3. *Description of the RO process in the hybrid FO-RO system*

The steady state model developed above for a spiral wound RO process will be used to build and characterize the complete modeling of the multi element RO process in the hybrid FO-RO system.

Fig. 1 shows the hybrid FO-RO system. The forward osmosis unit (1) consists of two channels having solutions of different concentrations, separated by a semipermeable FO membrane. The low concentration solution is called a feed solution and the high concentration solution is called a draw solution. In the FO process the initial draw solute concentration ($C_{ds,in}$) from the draw solution channel is diluted due to the pure water flux ($J_{w,\ FO}$) and reverse solute flux ($J_{s,\ FO}$) through the FO membrane (She et al., 2012). The pure water flux ($J_{w,\ FO}$) and reverse solute flux ($J_{s,\ FO}$) through the FO membrane change with the operating temperature of the FO process (Chowdhury and McCutcheon, 2018). Therefore, the diluted draw solution flow rate ($Q_{ds,\ out}$) and concentration ($C_{ds,\ out}$) from the outlet of the FO module may vary. The contaminant concentration in the diluted draw solution is very low because of good contaminant rejection by the FO membrane. (Irvine et al., 2013; Jang et al., 2018). The diluted draw solution therefore may be considered as a binary solution having very less concentration of contaminants. In this study, the diluted draw solution is sodium chloride solution. Since it is a non-scaling and non-fouling solute, the RO flow factor F_f assumed in this study is 0.977.

The role of the RO process in the FO-RO hybrid system is to regenerate the diluted draw solution coming from the FO

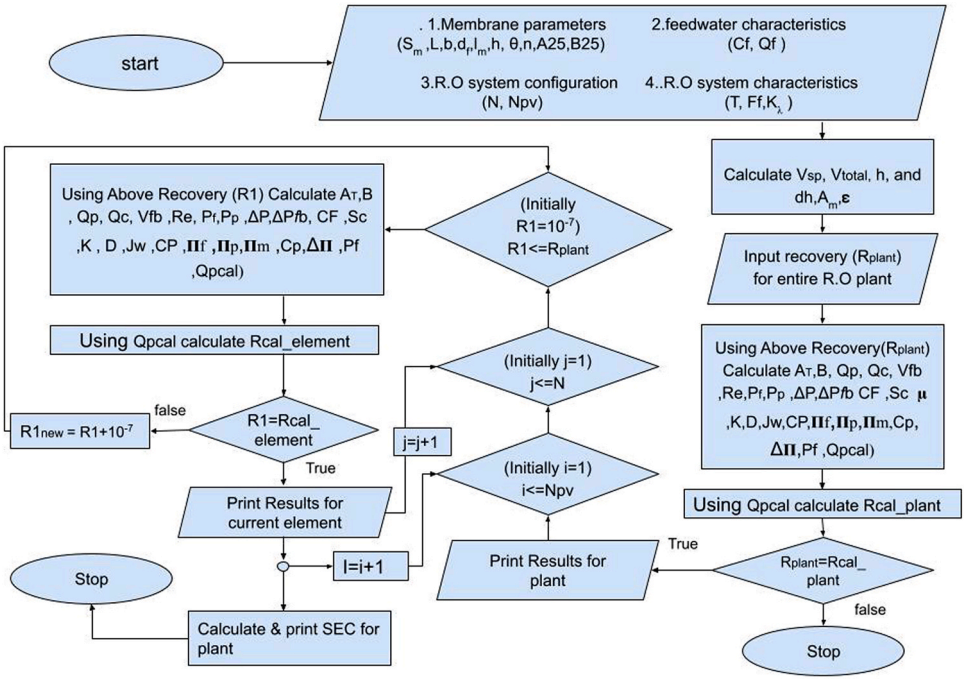

Fig. 2 – Flowchart of algorithm for multi element multi pressure vessel single stage RO system.

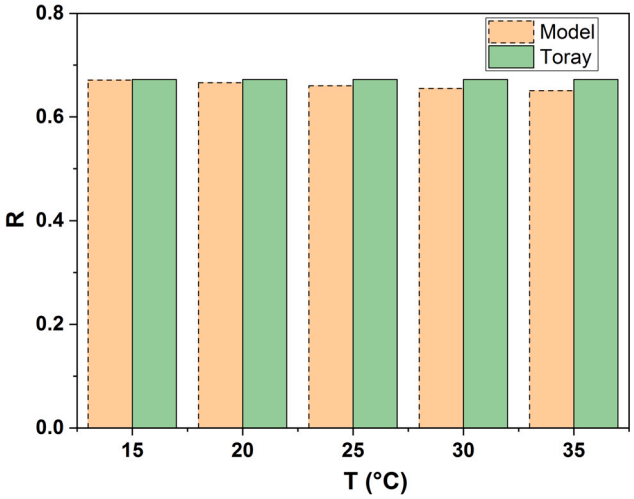

Fig. 3 – Model vs Toray results for RO plant recovery at varying temperatures (15 °C, 20 °C, 25 °C, 30 °C and 35 °C).

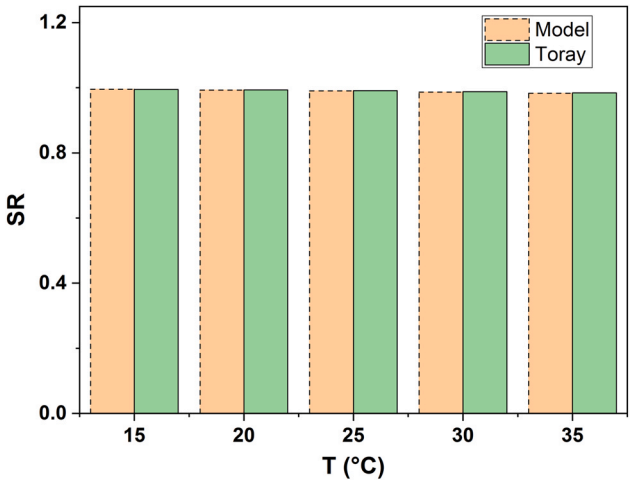

Fig. 4 – Model vs Toray results for salt rejection at varying temperatures (15 °C, 20 °C, 25 °C, 30 °C and 35 °C).

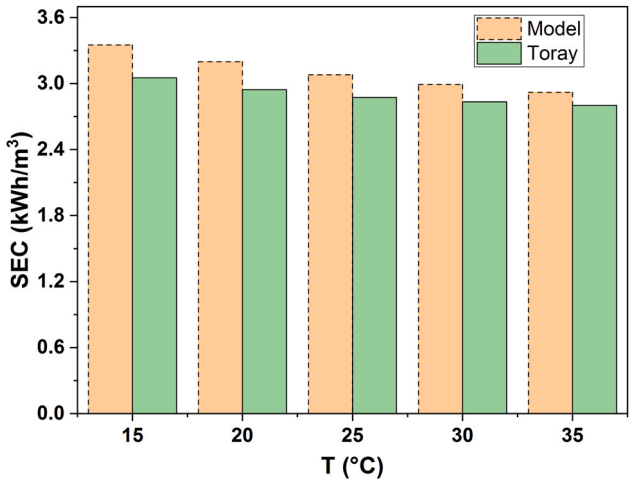

Fig. 5 – Model vs Toray results for RO plant specific energy consumption at varying temperatures (15 °C, 20 °C, 25 °C, 30 °C and 35 °C).

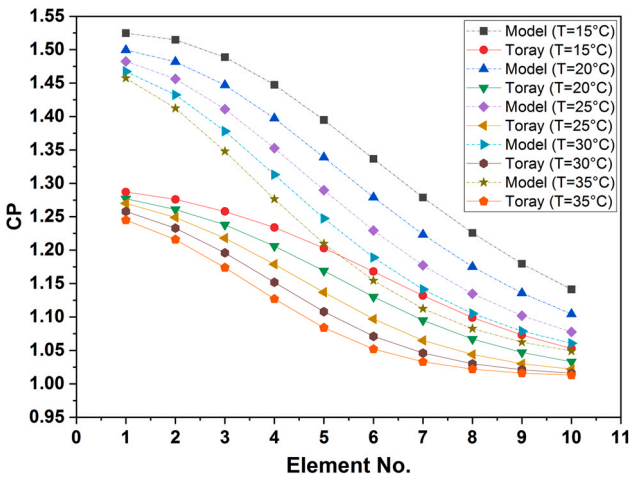

Fig. 6 – Concentration polarization along the length of the pressure vessel (15 °C, 20 °C, 25 °C, 30 °C and 35 °C).

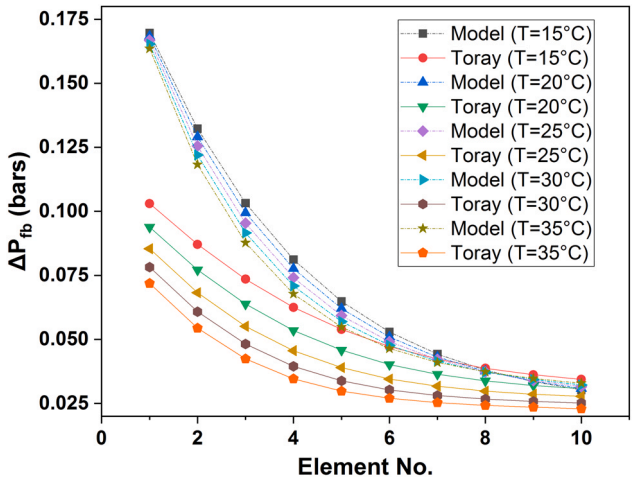

Fig. 7 – Pressure drop along the length of the pressure vessel at varying temperatures (15 °C, 20 °C, 25 °C, 30 °C and 35 °C).

process and resend it back to the FO process. The diluted draw solution coming from the FO process is collected in diluted draw solution tank (2) as shown in Fig. 1. The concentration in (2) is maintained by adding concentrated salt solution from the high concentration draw solution reservoir (3) with the help of a dosing pump (4) connected to a conductivity controller unit (5). From (2), at constant flow rate (Q_f) and at constant concentration (C_f) the salt solution as RO feedwater is fed to the RO membrane unit (6) process. The RO process is then run to regenerate the initial draw solution concentration ($C_{ds,\ in}$) through the RO concentrate stream.

The design of RO is focused on optimizing the RO concentrate concentration (C_c) and flow rate (Q_c) to maintain the performance of the FO process of the hybrid FO-RO system. The recovery rate of the RO process is assumed such that the RO plant specific energy consumption will be minimum. (Liu et al., 2012) reported that the minimum specific energy occurs beyond 60% when a RO channel is working in the mass transfer limited regime in which the osmotic pressure of the retentate by the exit end of the channel is much smaller than the driving pressure ΔP. Accordingly the recovery ratio R, for the RO process is fixed to 67.22% which is near to the minimum specific energy consumption. Table 2 shows the details of the RO feedwater fed to the RO plant, design specifications and plant operating conditions. A polyamide thin film composite spiral wound RO membrane (TM820M-400/SWRO) was chosen as the reverse osmosis membrane material in the present work. The details of the membrane characteristics and manufacturer established constraints are shown in Table 3.

2.4. *Model implementation in python*

Using the above equations, a model was developed using the Python computer language to determine the process performance of the multi element single stage RO process. Fig. 2 shows the flowchart of the developed program that presents the algorithm for a multi element single-stage reverse osmosis process. Python libraries used in this program are Math, Numpy and Gspread. To link the model to the Google spreadsheet, the Google Sheet API was utilized. Membrane characteristics data of TM820M-400/SWRO Toray membrane obtained from Al-Obaidi et al. (2019) was entered in the google spreadsheet. With the help of the gspread library the model was able to import various values of membrane characteristics from the google spreadsheet database after providing only membrane designation as input to the model.

The membrane configuration was selected by providing number of membrane elements and number of pressure vessels data to the model. The parameters as input to the model were membrane designation, RO feed water flowrate, concentration, temperature, RO recovery and flow factor. To determine the performance of a multi-element RO in a pressure vessel, element wise calculation required iteration. A simple iterative process is used to solve the iterations in python rather than using any numerical method or any other computational tool. "For" loop was used to perform the iterations. To solve any iteration initial guess is required. As a result, to initialize the simulation an initial guess for recovery embedded in the program was 1×10^{-7}.

The simulation is run and the results of the model are exported to the google spreadsheet. The results exceeding the membrane manufacturer laid constraints were highlighted with green color for ease of readability. To change the color of cells in a google spreadsheet, the "worksheet.format ()" function from the gspread library was used. Before starting the computation, the model changes the color of the cells to green. While plotting the results, if any parameter exceeds the set constraints, the model instantly changes the color of the cell to red.

3. Results and discussion

Using the model, simulation was carried out and the model's findings were compared with the results produced using Toray software (Toray, 2021) which is commercial RO design software. The input parameters for the model and Toray software are shown in Table 2. Due to the variation in fluid and membrane polymer characteristics at different temperatures, the performance of RO membranes is affected by the feed temperature (Shaaban and Yahya, 2017). During membrane testing, simulation results provided by model and Toray software have been obtained for 15 °C, 20 °C, 25 °C, 30 °C and 35 °C feed water temperatures.

Fig. 3 shows the model and Toray results for calculated recovery (R_{cal}) obtained at feed water temperature 15 °C, 20 °C, 25 °C, 30 °C and 35 °C respectively. The water recovery ratios of the model are lower than that of Toray software with a maximum error of 3.2% at 35 °C. For lower temperature, there was less difference between model and Toray software, while the error increased for higher temperature. Fig. 4 shows the model and Toray results for salt rejection (SR) obtained at feed water temperature 15 °C, 20 °C, 25 °C, 30 °C and 35 °C respectively. For increasing temperature there is a decrease in the salt rejection (Jiang et al., 2014). The salt rejection values of the model are in close agreement with the values of Toray software with a maximum error of 0.12% for temperature 30 °C and minimum error of 0.018% for temperature 15 °C. Fig. 5 shows the model and Toray results for specific energy consumption (SEC) obtained at feed water temperature 15 °C, 20 °C, 25 °C, 30 °C and 35 °C respectively. With increase in feed solution temperature there is a decrease in the SEC value for both the model and Toray software. The SEC values of the model are higher than that of Toray software with a maximum error of 9.76%. For higher temperature of feed water, there was less difference between

model and Toray software, while the error increased for lower temperature of RO feed water.

This difference in performance parameters is due to the difference in the equations used for parameter estimation by the model and the Toray software. In the model the sodium chloride solution parameters like viscosity, diffusion coefficient and density are determined as given by Eddouibi et al. (2021), whereas the Toray software does not display these parameters in their software result. These parameters are used to equate other parameters like concentration polarization and pressure drop along the length of the pressure vessel which largely affect the estimation of the RO performance parameters (Bartholomew and Mauter, 2019). The differences obtained in the results of the model and Toray for concentration polarization and pressure drop are discussed below.

Fig. 6 shows the model and Toray results for concentration polarization factor obtained along the length of the pressure vessel at feed water temperature 15 °C, 20 °C, 25 °C, 30 °C and 35 °C respectively. From the figure it can be seen that the concentration polarization values increase with respect to increase in temperature for both the model and Toray software. The CP in the pressure vessel decreases along the length of the membrane for the model and Toray software (Jiang et al., 2014). The CP values provided by Toray software are lower than that estimated by the model for temperature 15 °C, 20 °C, 25 °C, 30 °C and 35 °C respectively.

In this study the pressure drop along the length of the pressure vessel is calculated by equations provided by (Jiang et al., 2014; Ruiz-García and de la Nuez Pestana, 2019). The total pressure drop along the length of the membrane estimated by model at 15 °C, 20 °C, 25 °C, 30 °C and 35 °C, are 0.75, 0.73, 0.72, 0.7 and 0.68 bars respectively. The total pressure drop along the length of the membrane provided by Toray software at 15 °C, 20 °C, 25 °C, 30 °C and 35 °C, are 0.58, 0.51, 0.45, 0.4 and 0.36 bars respectively. The total pressure drop estimated by model is higher than the values estimated by Toray software. Fig. 7 shows the model and Toray results for the pressure drop along the length of the pressure vessel. From the figure it can easily be seen that the pressure drop decreases nonlinearly along the length of the pressure vessel for both the model and Toray software. The pressure drop in the pressure vessel decreases along the length of the pressure vessel with increasing feed water temperature for both the model and Toray software. The pressure drop values provided by Toray software are lower than that estimated by the model with a maximum difference of 0.328 bars for 35 °C.

The simple iterative method adopted in this study to estimate the RO performance parameters also induces difference in the results of the model. The equations describing the RO process model are solved iteratively. The calculation was initialized with a value of 1×10^{-7} as the initial value of element recovery embedded in the code of the Python program to obtain the results of the RO process parameters.

4. Conclusion

In this study the performance of the multi element single stage RO process in a hybrid FO-RO system was estimated using a model developed in python. The diluted draw solution concentration from the FO process is first adjusted to constant concentration and flowrate and then fed to the RO system as RO feedwater. The RO feed water is considered a binary solution (sodium chloride solution) and equations providing appropriate thermo-chemical properties of the RO feed water are incorporated in the developed RO model. The model is open to use with any make of spiral wound RO membrane and do simulation for varying temperature of RO feed water.

The model results were compared with Toray software for similar input criteria. The maximum difference in the recovery ratio between model and Toray software was 3.2% at 35 °C, which seems to be reasonably acceptable. The salt rejection values estimated by model are in good agreement with Toray software with a maximum error of 0.12% at 30 °C. The error in SEC between model predictions and Toray was minimum 4.24% at 35 °C and maximum 9.76% at 15 °C. The error in SEC becomes increasingly important as it is the most important parameter for cost evaluation of the RO system.

The maximum pressure drop difference between the model and the Toray software is 0.328 bars for 35 °C. The error induced in results because of this difference is negligible so pressure drop difference between the model and Toray software is in good agreement. Model prediction error for SEC seems to be higher because of the difference in concentration polarization and pressure drop predictions between model and Toray. The maximum and minimum difference in the concentration polarization between model and Toray software was 18.46% at 15 °C and 3.56% at 35 °C respectively. This difference may be because equations assigned for calculating mass transfer coefficient (k) in model and Toray software are different. Further studies will be required to experimentally validate the model. This might increase the application of this model in estimating performance parameters of RO step in the FO-RO process and help in accurate cost estimation of hybrid FO-RO systems.

Declaration of Competing Interest

The authors declare that they have no known competing financial interests or personal relationships that could have appeared to influence the work reported in this paper.

Acknowledgments

SUS and NKK wish to acknowledge the support received from Civil and Environmental Engineering Department, VJTI, Mumbai, MH, India for this research work. SMS wish to acknowledge the support received from Department of Civil Engineering, Dr. B.A.T.U, Vidyavihar, Lonere, MH, INDIA for this research work.

References

Achilli, A., Cath, T.Y., Childress, A.E., 2010. Selection of inorganic-based draw solutions for forward osmosis applications. J. Membr. Sci. 364 (1–2), 233–241. https://doi.org/10.1016/j.memsci.2010.08.010

Ali, H.M., Gadallah, H., Ali, S.S., Sabry, R., Gadallah, A.G., 2016. Pilot-scale investigation of forward/reverse osmosis hybrid system for seawater desalination using impaired water from steel industry. Int. J. Chem. Eng. 2016, 1–9. https://doi.org/10.1155/2016/8745943

Al-Obaidi, M.A., Alsarayreh, A.A., Al-Hroub, A.M., Alsadaie, S., Mujtaba, I.M., 2018. Performance analysis of a medium-sized industrial reverse osmosis brackish water desalination plant. Desalination 443, 272–284. https://doi.org/10.1016/j.desal.2018.06.010

Al-Obaidi, M.A., Filippini, G., Manenti, F., Mujtaba, I.M., 2019. Cost evaluation and optimisation of hybrid multi effect distillation and reverse osmosis system for seawater desalination. Desalination 456, 136–149. https://doi.org/10.1016/j.desal.2019.01.019

Al-Obaidi, M.A., Ruiz-García, A., Hassan, G., Li, J.-P., Kara-Zaïtri, C., Nuez, I., Mujtaba, I.M., 2021. Model based simulation and genetic algorithm based optimisation of spiral wound membrane RO process for improved dimethylphenol rejection from wastewater. Membranes 11 (595), 19. https://doi.org/10.3390/membranes11080595

Altaee, A., 2012. Computational model for estimating reverse osmosis system design and performance: Part-one binary feed solution. Desalination 291, 101–105. https://doi.org/10.1016/j.desal.2012.01.028

Altaee, A., Millar, G.J., Zaragoza, G., Sharif, A., 2017. Energy efficiency of RO and FO–RO system for high-salinity seawater treatment. Clean. Technol. Environ. Policy 19 (1), 77–91. https://doi.org/10.1007/s10098-016-1190-3

Al-Zuhairi, A., Merdaw, A.A., Al-Aibi, S., Hamdan, M., Nicoll, P., Monjezi, A.A., Al-ASwad, S., Mahood, H.B., Aryafar, M., Sharif, A.O., 2015. Forward osmosis desalination from laboratory to market. Water Supply 15 (4), 834–844. https://doi.org/10.2166/ws.2015.038

Askari, M., Liang, C.Z., Choong, L.T., (Simon), Chung, T.-S., 2021. Optimization of TFC-PES hollow fiber membranes for reverse osmosis (RO) and osmotically assisted reverse osmosis (OARO) applications. J. Membr. Sci. 625, 119156. https://doi.org/10.1016/j.memsci.2021.119156

Bamaga, O.A., Yokochi, A., Zabara, B., Babaqi, A.S., 2011. Hybrid FO/RO desalination system: Preliminary assessment of osmotic energy recovery and designs of new FO membrane module configurations. Desalination 268 (1–3), 163–169. https://doi.org/10.1016/j.desal.2010.10.013

Bartholomew, T.V., Mauter, M.S., 2019. Computational framework for modeling membrane processes without process and solution property simplifications. J. Membr. Sci. 573, 682–693. https://doi.org/10.1016/j.memsci.2018.11.067

Bowden, K.S., Achilli, A., Childress, A.E., 2012. Organic ionic salt draw solutions for osmotic membrane bioreactors. Bioresour. Technol. 122, 207–216. https://doi.org/10.1016/j.biortech.2012.06.026

Brião, V.B., Magoga, J., Hemkemeier, M., Brião, E.B., Girardelli, L., Sbeghen, L., Favaretto, D.P.C., 2014. Reverse osmosis for desalination of water from the Guarani Aquifer System to produce drinking water in southern Brazil. Desalination 344, 402–411. https://doi.org/10.1016/j.desal.2014.04.008

Choi, B.G., Kim, D.I., Hong, S., 2016. Fouling evaluation and mechanisms in a FO-RO hybrid process for direct potable reuse. J. Membr. Sci. 520, 89–98. https://doi.org/10.1016/j.memsci.2016.07.035

Chowdhury, M.R., McCutcheon, J.R., 2018. Elucidating the impact of temperature gradients across membranes during forward osmosis: Coupling heat and mass transfer models for better prediction of real osmotic systems. J. Membr. Sci. 553, 189–199. https://doi.org/10.1016/j.memsci.2018.01.004

Chun, Y., Zaviska, F., Kim, S.-J., Mulcahy, D., Yang, E., Kim, I.S., Zou, L., 2016. Fouling characteristics and their implications on cleaning of a FO-RO pilot process for treating brackish surface water. Desalination 394, 91–100. https://doi.org/10.1016/j.desal.2016.04.026

Colla, V., Branca, T.A., Rosito, F., Lucca, C., Vivas, B.P., Delmiro, V.M., 2016. Sustainable Reverse Osmosis application for wastewater treatment in the steel industry. J. Clean. Prod. 130, 103–115. https://doi.org/10.1016/j.jclepro.2015.09.025

Cornelissen, E.R., Harmsen, D.J.H., Blankert, B., Wessels, L.P., van der Meer, W.G.J., 2021. Effect of minimal pre-treatment on reverse osmosis using surface water as a source. Desalination 509, 115056. https://doi.org/10.1016/j.desal.2021.115056

Dimitriou, E., Boutikos, P., Mohamed, E.Sh, Koziel, S., Papadakis, G., 2017. Theoretical performance prediction of a reverse osmosis desalination membrane element under variable operating conditions. Desalination 419, 70–78. https://doi.org/10.1016/j.desal.2017.06.001

Eddouibi, J., Abderafi, S., Vaudreuil, S., Bounahmidi, T., 2021. Water desalination by forward osmosis: Dynamic performance assessment and experimental validation using MgCl2 and NaCl as draw solutes. Comput. Chem. Eng. 149, 107313. https://doi.org/10.1016/j.compchemeng.2021.107313

Fritzmann, C., Löwenberg, J., Wintgens, T., Melin, T., 2007. State-of-the-art of reverse osmosis desalination. Desalination 216 (1–3), 1–76. https://doi.org/10.1016/j.desal.2006.12.009

Gaublomme, D., Strubbe, L., Vanoppen, M., Torfs, E., Mortier, S., Cornelissen, E., De Gusseme, B., Verliefde, A., Nopens, I., 2020. A generic reverse osmosis model for full-scale operation. Desalination 490, 114509. https://doi.org/10.1016/j.desal.2020.114509

Hao, Z., Zhao, S., Li, Q., Wang, Y., Zhang, J., Wang, Z., Wang, J., 2021. Reverse osmosis membranes with sulfonate and phosphate groups having excellent anti- scaling and anti-fouling properties. Desalination 509 (115076), 10. https://doi.org/10.1016/j.desal.2021.115076

Irvine, G.J., Rajesh, S., Georgiadis, M., Phillip, W.A., 2013. Ion selective permeation through cellulose acetate membranes in forward osmosis. Environ. Sci. Technol. 47 (23), 13745–13753. https://doi.org/10.1021/es403581t

Jamaly, S., Darwish, N.N., Ahmed, I., Hasan, S.W., 2014. A short review on reverse osmosis pretreatment technologies. Desalination 354, 30–38. https://doi.org/10.1016/j.desal.2014.09.017

Jang, D., Jeong, S., Jang, A., Kang, S., 2018. Relating solute properties of contaminants of emerging concern and their rejection by forward osmosis membrane. Sci. Total Environ. 639, 673–678. https://doi.org/10.1016/j.scitotenv.2018.05.078

Jeon, J., Park, B., Yoon, Y., Kim, S., 2016. An optimal design approach of forward osmosis and reverse osmosis hybrid process for seawater desalination. Desalin. Water Treat. 57 (55), 26612–26620. https://doi.org/10.1080/19443994.2016.1189701

Jeong, K., Son, M., Yoon, N., Park, S., Shim, J., Kim, J., Lim, J.-L., Cho, K.H., 2021. Modeling and evaluating performance of full-scale reverse osmosis system in industrial water treatment plant. Desalination 518, 115289. https://doi.org/10.1016/j.desal.2021.115289

Jiang, A., Ding, Q., Wang, J., Jiangzhou, S., Cheng, W., Xing, C., 2014. Mathematical Modeling and Simulation of SWRO Process Based on Simultaneous Method. J. Appl. Math. 2014, 1–11. https://doi.org/10.1155/2014/908569

Joshi, S.V., Ghosh, P.K., Shah, V.J., Devmurari, C.V., Trivedi, J.J., Rao, P., 2004. CSMCRI experience with reverse osmosis membranes and desalination: Case studies. Desalination 165, 201–208. https://doi.org/10.1016/j.desal.2004.06.023

Khraisheh, M., Dawas, N., Nasser, M.S., Al-Marri, M.J., Hussien, M.A., Adham, S., McKay, G., 2020. Osmotic pressure estimation using the Pitzer equation for forward osmosis modelling. Environ. Technol. 41 (19), 2533–2545. https://doi.org/10.1080/09593330.2019.1575476

Koroneos, C., Dompros, A., Roumbas, G., 2007. Renewable energy driven desalination systems modelling. J. Clean. Prod. 15 (5), 449–464. https://doi.org/10.1016/j.jclepro.2005.07.017

Lakho, F.H., Le, H.Q., Mattheeuws, F., Igodt, W., Depuydt, V., Desloover, J., Rousseau, D.P.L., Van Hulle, S.W.H., 2021. Decentralized grey and black water reuse by combining a vertical flow constructed wetland and membrane based potable water system: Full scale demonstration. J. Environ. Chem. Eng. 9 (1), 104688. https://doi.org/10.1016/j.jece.2020.104688

Lee, S., Boo, C., Elimelech, M., Hong, S., 2010. Comparison of fouling behavior in forward osmosis (FO) and reverse osmosis (RO). J. Membr. Sci. 365 (1–2), 34–39. https://doi.org/10.1016/j.memsci.2010.08.036

Liang, C.Z., Askari, M., Tchuin, L., Chung, T.-S., 2021. Ultra-strong polymeric hollow fiber membranes for saline dewatering and desalination. Nat. Commun. 12 (2338), 13. https://doi.org/10.1038/s41467-021-22684-1

Liu, C., Rainwater, K., Song, L., 2012. Calculation of energy consumption for crossflow RO desalination processes. Desalin. Water Treat. 42 (1–3), 295–303. https://doi.org/10.1080/19443994.2012.683138

Mancha, E., DeMichele, D., Walker, W.S., Seacord, T.F., Sutherland, J., Cano, A., 2014. Perform. Eval. Reverse Osmosis Membr. Comput. Models 89.

McCutcheon, J.R., McGinnis, R.L., Elimelech, M., 2006. Desalination by ammonia–carbon dioxide forward osmosis: Influence of draw and feed solution concentrations on process performance. J. Membr. Sci. 278 (1–2), 114–123. https://doi.org/10.1016/j.memsci.2005.10.048

Melián-Martel, N., Sadhwani Alonso, J.J., Ruiz-García, A., 2018. Combined silica and sodium alginate fouling of spiral-wound reverse osmosis membranes for seawater desalination. Desalination 439, 25–30. https://doi.org/10.1016/j.desal.2018.03.032

Nafey, A.S., Fath, H.E.S., Mabrouk, A.A., 2006. A new visual package for design and simulation of desalination processes. Desalination 194 (1–3), 281–296. https://doi.org/10.1016/j.desal.2005.09.032

Pais, J.A.G.C.R., Ferreira, L.M.G.A., 2007. Performance study of an industrial RO plant for seawater desalination. Desalination 208 (1–3), 269–276. https://doi.org/10.1016/j.desal.2006.06.017

Park, P.-K., Lee, S., Cho, J.-S., Kim, J.-H., 2012. Full-scale simulation of seawater reverse osmosis desalination processes for boron removal: Effect of membrane fouling. Water Res. 46 (12), 3796–3804. https://doi.org/10.1016/j.watres.2012.04.021

Qin, J.-J., Htun Oo, M., Nyunt Wai, M., Lee, H., Hong, S.P., Kim, J.E., Xing, Y., Zhanga, M., 2005. Pilot study for reclamation of secondary treated sewage effluent. Desalination 171 (3), 299–305. https://doi.org/10.1016/j.desal.2004.05.008

Rahimi, B., Afzali, M., Farhadi, F., Alamolhoda, A.A., 2021. Reverse osmosis desalination for irrigation in a pistachio orchard. Desalination 516, 115236. https://doi.org/10.1016/j.desal.2021.115236

Ruiz-García, A., de la Nuez Pestana, I., 2019. Feed spacer geometries and permeability coefficients. Effect on the performance in BWRO spriral-wound membrane modules. Water 11 (1), 152. https://doi.org/10.3390/w11010152

Ruiz-García, A., Nuez, I., 2016. Long-term performance decline in a brackish water reverse osmosis desalination plant. Predictive model for the water permeability coefficient. Desalination 397, 101–107. https://doi.org/10.1016/j.desal.2016.06.027

Ruiz-García, A., Nuez-Pestana, I. de la, 2018. A computational tool for designing BWRO systems with spiral wound modules. Desalination 426, 69–77. https://doi.org/10.1016/j.desal.2017.10.040

Ruiz-García, A., Nuez, I., Carrascosa-Chisvert, M., Santana, J.J., 2020. Simul. BWRO Syst. Differ. Feed. Charact. Anal. Oper. Windows Optim. Oper. Points 491 (114582), 9. https://doi.org/10.1016/j.desal.2020.114582

Shaaban, S., Yahya, H., 2017. Detailed analysis of reverse osmosis systems in hot climate conditions. Desalination 423, 41–51. https://doi.org/10.1016/j.desal.2017.09.002

She, Q., Jin, X., Li, Q., Tang, C.Y., 2012. Relating reverse and forward solute diffusion to membrane fouling in osmotically driven membrane processes. Water Res. 46 (7), 2478–2486. https://doi.org/10.1016/j.watres.2012.02.024

Shock, G., Miquel, A., 1987. Mass Transfer and Pressure loss in Spiral Wound Modules. Desalination 64, 339–352.

Thiruvenkatachari, R., Francis, M., Cunnington, M., Su, S., 2016. Application of integrated forward and reverse osmosis for coal mine wastewater desalination. Sep. Purif. Technol. 163, 181–188. https://doi.org/10.1016/j.seppur.2016.02.034

Toray, 2021. *Toray Design System 2.0* (2.2.3.199) [Computer software]. Toray Industries, Inc.,. ⟨https://www.water.toray/knowledge/tool/ds/⟩.

Wijmans, J.G., Baker, R.W., 1995. The solution-diffusion model: A review. J. Membr. Sci. 107 (1–2), 1–21. https://doi.org/10.1016/0376-7388(95)00102-I

Yangali-Quintanilla, V., Li, Z., Valladares, R., Li, Q., Amy, G., 2011. Indirect desalination of Red Sea water with forward osmosis and low pressure reverse osmosis for water reuse. Desalination 280 (1–3), 160–166. https://doi.org/10.1016/j.desal.2011.06.066

Zaviska, F., Chun, Y., Heran, M., Zou, L., 2015. Using FO as pretreatment of RO for high scaling potential brackish water: Energy and performance optimisation. J. Membr. Sci. 492, 430–438. https://doi.org/10.1016/j.memsci.2015.06.004